THE JOURNAL OF PHYSICAL CHEMISTRY A

Article

Cite This: J. Phys. Chem. A 2017, 121, 9495−9507

pubs.acs.org/JPCA

Dispersion Interactions in QM/EFP

Lyudmila V. Slipchenko,*[,†] Mark S. Gordon,[‡] and Klaus Ruedenberg[‡]

[†]Department of Chemistry, Purdue University, West Lafayette, Indiana 47907, United States

[‡]Department of Chemistry and Ames Laboratory, Iowa State University, Ames, Iowa 50011, United States

Supporting Information

ABSTRACT: The dispersion energy term between quantum-mechanical (QM) and classical (represented by effective fragment potentials, EFP) subsystems is developed and implemented. A new formulation is based on long-range perturbation theory and uses dynamic polarizability tensors of the effective fragments and electric field integrals and orbital energies of the quantum-mechanical subsystem. No parametrization is involved. The accuracy of the QM−EFP dispersion energy is tested on a number of model systems; the average mean unsigned error is 0.8 kcal/mol or 13% with respect to the symmetry adapted perturbation theory on the S22 data set of noncovalent interactions. The computational cost of the dispersion energy computation is low compared to the self-consistent field calculation of the QM subsystem. The dispersion energy is sensitive to the level of theory employed for the QM part and to the electrostatic interactions in the system. The latter means that the dispersion interactions in the QM/EFP method are not purely two-body but have more complex many-body behavior.

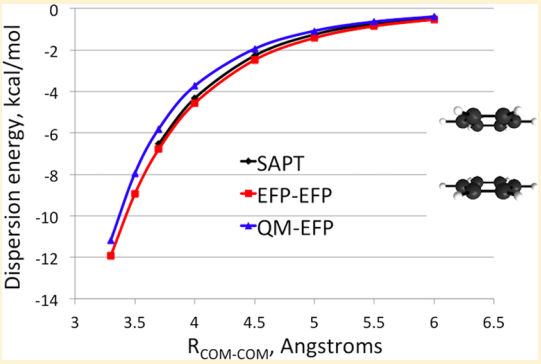

1. INTRODUCTION

Computationally efficient but physically rigorous modeling of molecular systems is a goal that has driven algorithmic and methodological advances since the emergence of the first computers. One popular direction along this route is to develop model Hamiltonians that effectively separate both time and length scales of a complex chemical event into local events. The Born−Oppenheimer approximation is one example of this general approach applied for separation of time scales. Fragmentation and QM/MM models for extended molecular systems provide successful examples in which the separation of length scales dramatically lowers the computational cost.[1−3] The latter methods are based on the idea that molecular interactions are separable into short and long-range, and as such, can be modeled with different Hamiltonians. Long-range interactions are further separated into electrostatic and van der Waals terms, and both attract massive theoretical effort, including recent developments in embedding schemes and dispersion corrections in density functional methods.[4−18] This work reports a new formulation of the dispersion energy in a hybrid quantum-classical system, where the classical subsystem is described with effective fragment potentials (EFP).[19−23] The developed formalism is based on a quantum-mechanical description of the dispersion and does not include parametrization of either quantum or EFP subsystems.

The EFP method[19−23] has emerged as a rigorous way to evaluate interactions between noncovalently bound fragments. The EFP method is one of a few available general polarizable potentials, with the highly parametrized AMOEBA,[24] SIBFA,[25,26] and several others[11,27−29] also becoming increasingly popular. Long-range perturbation theory is used to derive expressions for Coulomb (electrostatics), polarization (induction), and dispersion terms in the EFP method. The short-range terms, exchange-repulsion and charge-transfer, are obtained as truncated expansions in powers of intermolecular overlap. A distributed approach is used throughout the EFP derivation. For example, multipoles for the Coulomb term are centered at atoms and bond-midpoints, and the static and dynamic polarizability tensors (for calculating polarization and dispersion interactions, respectively) are obtained at the points corresponding to centers of localized orbitals. A localized wave function on each fragment is used for modeling exchange-repulsion interactions. Parameters for each term in the EFP interaction energy are obtained from a set of *ab initio* calculations on each unique fragment; for convenience and reproducibility of the results, these parameters are stored in an open-access EFP parameter library.[30] Coulomb, polarization, and dispersion terms are augmented by damping functions that accurately capture the short-range charge-penetration effects and prevent instabilities in polarization interactions.[31] The uniqueness of the EFP method is that *all effective fragment parameters are derived from first-principles*, i.e., the method does not require cumbersome and often equivocal fitting of parameters.

The EFP method can be combined with a quantum subsystem in QM/MM calculations that can be used to model processes involving electronic redistribution such as chemical reactions, electronic excitations, energy and/or

Received: June 15, 2017
Revised: November 7, 2017
Published: November 9, 2017

DOI: 10.1021/acs.jpca.7b05875
J. Phys. Chem. A 2017, 121, 9495−9507

electron transfer. Various QM/MM methods[2,3,32−42] have been developed since the initial work of Warshel,[42] including multilayer methods such as ONIOM,[43−45] Truhlar MCMM methods[46,47] and polarizable QM/MM for linear response methods by Kongsted and co-workers.[11,27] The Hamiltonian of the QM/MM system consists of three terms:

$$\hat{H} = \hat{H}_{\mathrm{QM}} + \hat{H}_{\mathrm{MM}} + \hat{H}_{\mathrm{QM-MM}} \tag{1}$$

where $\hat{H}_{\mathrm{QM\text{-}MM}}$ is a coupling term. Separation of the QM and MM subsystems, in principle, allows one to use any level of theory in both the QM and MM parts. In the context of this work, $\hat{H}_{MM}$ is the EFP Hamiltonian. Then, following the EFP energy components, $\hat{H}_{\mathrm{QM-EFP}}$ can be represented as

$$\hat{H}_{\mathrm{QM-EFP}} = \hat{H}^{\mathrm{Coul}} + \hat{H}^{\mathrm{pol}} + \hat{H}^{\mathrm{disp}} + \hat{H}^{\mathrm{exrep}} + \hat{H}^{\mathrm{CT}} \tag{2}$$

In the present work, the last term (charge transfer) is not included. Electrostatic and polarization contributions to $\hat{H}_{\mathrm{QM-EFP}}$ ($\hat{H}^{\mathrm{Coul}}$ and $\hat{H}^{\mathrm{pol}}$) are added as one-electron terms to the quantum Hamiltonian, defining a polarizable embedding scheme. The computational cost associated with the inclusion of these terms is minor with respect to the cost of the gas phase QM computation, at least for small fragments and if the number of effective fragments is no more than a few thousand.

In a typical QM/MM scheme, the dispersion and exchange-repulsion interactions are combined in a van der Waals term that is parametrized within a Lennard-Jones (LJ) potential and included in $\hat{H}_{\mathrm{QM-MM}}$ at the MM level. However, the LJ parameters of the QM subsystem may become inaccurate during a chemical reaction or electronic redistribution, since these parameters are fixed. Additionally, the electronic wave function and electronic density of the QM subsystem are completely unaffected by LJ interactions with the solvent. The latter deficiency becomes evident in the inability of classical QM/MM approaches to describe solvatochromic shifts in nonpolar solvents and shifts of Rydberg states that are governed by short-range cavity effects.[48,49]

The current work describes a new implementation of the QM−EFP dispersion term. This implementation addresses the main deficiencies of modeling dispersion interactions in LJ-based QM/MM schemes while conserving the computational efficiency of the QM/EFP approach.

2. THEORY

EFP−EFP Dispersion Energy. Starting from Rayleigh−Schrödinger second-order perturbation theory, the dispersion energy between molecules A and B is[50]

$$E^{\mathrm{disp}} = -\sum_{m\neq 0, n\neq 0} \frac{\langle 00|\hat{H}'|mn\rangle\langle mn|\hat{H}'|00\rangle}{W_m^{\mathrm{A}} + W_n^{\mathrm{B}} - W_0^{\mathrm{A}} - W_0^{\mathrm{B}}} \tag{3}$$

where m and n are states of molecules A and B, respectively, and the subscript 0 corresponds to the ground state. W_x^Y is the energy of molecule Y in state x. Formally, the dispersion energy in eq 3 corresponds to the $E^{(2)}_{\mathrm{disp}}$ term as defined in symmetry-adapted perturbation theory (SAPT) and other perturbation schemes. H' is the perturbed Hamiltonian generally expressed as

$$\hat{H}' = \int \frac{\hat{\rho}^A(r)\hat{\rho}^B(r')}{4\pi\varepsilon_0|r - r'|}\,\mathrm{d}r\,\mathrm{d}r' \tag{4}$$

where $\hat{\rho}^{A/B}(r)$ is a charge density operator for molecule A/B. When the interaction of two classical fragments is considered, the multipole expansion can be applied to the charge densities $\hat{\rho}^A$ and $\hat{\rho}^B$ such that $\hat{H}'$ becomes

$$\hat{\mathrm{H}}' = T\hat{q}^{\mathrm{A}}\hat{q}^{\mathrm{B}} + T_\alpha(\hat{q}^{\mathrm{A}}\hat{\mu}_\alpha^{\mathrm{B}} - \hat{\mu}_\alpha^{\mathrm{A}}\hat{q}^{B}) - T_{\alpha\beta}\hat{\mu}_\alpha^{\mathrm{A}}\hat{\mu}_\beta^{\mathrm{B}} + \ldots \tag{5}$$

T, T_α, and $T_{\alpha\beta}$ are the electrostatic tensors of zero, first, and second rank, respectively, that correspond to a Taylor expansion of $(1/R)$, i.e.:

$$T = \frac{1}{R} \tag{6a}$$

$$T_\alpha = \nabla_\alpha\left(\frac{1}{R}\right) = -\frac{R_\alpha}{R^3} \tag{6b}$$

$$T_{\alpha\beta} = \nabla_\beta\nabla_\alpha\left(\frac{1}{R}\right) = \frac{3R_\alpha R_\beta - R^2\delta_{\alpha\beta}}{R^5} \tag{6c}$$

$\hat{\mathrm{q}}^{\mathrm{A/B}}$ are charge and $\hat{\mu}^{\mathrm{A/B}}$ are dipole moment operators of fragments A or B. Here and below, subscripts α, β, etc denote x, y, z components of vector and tensor objects. Note that all terms with $\hat{q}^{\mathrm{A/B}}$ vanish in the dispersion energy expression eq 3 due to the orthogonality of different eigenstates of the Hamiltonian. Thus, the first and leading term in eq 5 that contributes to the dispersion energy is the dipole−dipole term:

$$\hat{\mathrm{H}}' = -T_{\alpha\beta}\hat{\mu}_\alpha^{\mathrm{A}}\hat{\mu}_\beta^{\mathrm{B}} \tag{7}$$

Substituting $\hat{H}'$ from eq 7 into eq 3 and assuming separability of the states on different molecules, $|mn\rangle = |m\rangle|n\rangle$, results in

$$E^{\mathrm{disp}} = -\sum_{m\neq 0, n\neq 0} T_{\alpha\beta}^{\mathrm{AB}} T_{\gamma\delta}^{\mathrm{AB}} \frac{\langle 0^{\mathrm{A}}|\hat{\mu}_\alpha^{\mathrm{A}}|m\rangle\langle m|\hat{\mu}_\gamma^{\mathrm{A}}|0^{\mathrm{A}}\rangle\langle 0^{\mathrm{B}}|\hat{\mu}_\beta^{\mathrm{B}}|n\rangle\langle n|\hat{\mu}_\delta^{\mathrm{B}}|0^{\mathrm{B}}\rangle}{E_{m0}^{\mathrm{A}} + E_{n0}^{\mathrm{B}}} \tag{8}$$

where $E_{\mathrm{X0}}^Y = W_X^Y - W_0^Y$ is the excitation energy of state X of molecule Y. Further, introducing the McLachlan identity:[50,51]

$$\frac{1}{A+B} = \frac{2}{\pi}\int_0^\infty \frac{AB}{(A^2+\omega^2)(B^2+\omega^2)}\,\mathrm{d}\omega \tag{9}$$

and the notation for the dynamic polarizability tensor $\alpha_{\alpha\beta}(\omega)$:

$$\alpha_{\alpha\beta}(\omega) = 2\sum_m \frac{\omega_{m0}\langle 0|\hat{\mu}_\alpha|m\rangle\langle m|\hat{\mu}_\beta|0\rangle}{\hbar(\omega_{m0}^2 - \omega^2)} \tag{10}$$

one comes to the principal expression for the first (E_6) term in the dispersion energy between molecules A and B:

$$E_6^{\mathrm{disp}} = -\frac{1}{2\pi}\sum_{\alpha\beta\gamma\delta}^{x,y,z} T_{\alpha\beta}^{\mathrm{AB}} T_{\gamma\delta}^{\mathrm{AB}} \int_0^\infty \alpha_{\alpha\gamma}^{\mathrm{A}}(i\omega)\alpha_{\beta\delta}^{\mathrm{B}}(i\omega)\,\mathrm{d}\omega \tag{11}$$

In the EFP method, eq 11 is further evolved by introducing a distributed approach (distributed points k and j on fragments A and B, respectively) and diagonal and isotropic approximations for the distributed dynamic polarizabilities $\bar{\alpha} = \frac{1}{3}(\alpha_{xx} + \alpha_{yy} + \alpha_{zz})$, resulting in the following dispersion energy expression:[52]

$$E_{\mathrm{EFP-EFP}}^{\mathrm{disp}} = -\frac{3}{\pi}\sum_{k\in A}\sum_{j\in B}\frac{1}{R_{kj}^6}\int_0^\infty \bar{\alpha}^k(i\omega)\bar{\alpha}^j(i\omega)\,\mathrm{d}\omega \tag{12}$$

Dynamic polarizabilities are distributed over localized molecular orbitals represented by points k and j in eq 12. R_{kj} is the distance between points k and j. The integral over imaginary frequencies in eq 12 is efficiently evaluated using a 12-point Gauss-Legendre quadrature and does not impose a

DOI: 10.1021/acs.jpca.7b05875
J. Phys. Chem. A 2017, 121, 9495−9507

significant computational cost. In the expression (12), the integral over dynamic polarizability tensors serves as an effective C_6 coefficient between each pair of fragments distributed polarizability points, $C_6^{kj} = \frac{3}{\pi}\int_0^\infty \bar{\alpha}^k(i\omega)\bar{\alpha}^j(i\omega)\,d\omega$. Additionally, screening functions f_6^{kj} between pairs of polarizability points are introduced to account for short-range exchange-dispersion mixing. Overlap-based screening functions are used as a default option.[31,53] In order to capture higher-order dispersion terms (C_7, C_8, etc.), the dispersion energy eq 12 is scaled by a coefficient 4/3. The recent development of the C_7 term[54] and work-in-progress on the C_8 term will hopefully eliminate the need for this somewhat arbitrary scaling factor. Therefore, the working expression for the dispersion energy between the EFP fragments is

$$E^{\mathrm{disp}}_{\mathrm{EFP-EFP}} = -\frac{4}{3}\sum_{k\in A, j\in B}\frac{f_6^{kj}C_6^{kj}}{R_{kj}^6} \tag{13}$$

QM−EFP Dispersion Energy. To obtain the expression for the dispersion energy between the QM and EFP subsystems, one needs to consider a mixed Hamiltonian in which only the EFP part is expanded in a multipole series, while the QM part is described by the electron density. This procedure results in the following form of the QM−EFP interaction Hamiltonian:

$$\hat{H}' = \int T_\alpha^{\mathrm{B}}(r)\hat{\mu}_\alpha^{\mathrm{B}}\hat{\rho}^{\mathrm{A}}(r)\,dr \tag{14}$$

Here molecule A is described quantum-mechanically and molecule B is an EFP fragment. The electrostatic tensor $T_\alpha^{\mathrm{B}}(r) = -\frac{(r-R^{\mathrm{B}})_\alpha}{(|r-R^{\mathrm{B}}|)^3}$ is computed between electronic coordinate r of the QM part and a distributed point at EFP fragment B. Again, the terms with $\hat{q}^{\mathrm{B}}$ do not enter the expression due to the orthogonality of the eigenstates on each molecule, and higher-order multipole terms are neglected.

By inserting the interaction Hamiltonian into the general expression for the dispersion energy eq 3, one obtains

$$E^{\mathrm{disp}} = -\sum_{m\neq 0, n\neq 0}\int dr\,dr' \frac{\langle 0|T_\alpha^{\mathrm{B}}(r)\hat{\rho}^{\mathrm{A}}(r)|m\rangle\langle m|T_\beta^{\mathrm{B}}(r')\hat{\rho}^{\mathrm{A}}(r')|0\rangle\langle 0|\hat{\mu}_\alpha^{\mathrm{B}}|n\rangle\langle n|\hat{\mu}_\beta^{\mathrm{B}}|0\rangle}{E_{m0}^{\mathrm{A}} + E_{n0}^{\mathrm{B}}} \tag{15}$$

Following the same strategy that was used to derive the fragment-fragment dispersion energy, i.e., by employing the McLachlan equality and combining the dipole moment integrals into dynamic polarizabilities, one can obtain the principal expression for the QM/EFP dispersion energy:

$$E^{\mathrm{disp}}_{\mathrm{QM-EFP}} = -\frac{1}{\pi}\sum_{m\neq 0}\sum_{\alpha\beta}^{x,y,z}\int dr\,dr'\langle 0|T_\alpha^{\mathrm{B}}(r)\hat{\rho}^{A}(r)|m\rangle\langle m|T_\beta^{\mathrm{B}}(r')\hat{\rho}^{A}(r')|0\rangle \int_0^\infty \frac{\omega_{m0}^{\mathrm{A}}}{(\omega_{m0}^{\mathrm{A}})^2+\omega^2}\alpha_{\alpha\beta}^{\mathrm{B}}(i\omega)\,d\omega \tag{16}$$

where ω_{m0}^A are energy differences between states 0 and m of the QM subsystem.

In spirit of the EFP methodology, distributed polarizability tensors on each fragment can be introduced. Additionally, the sum-over-states expression in eq 16 can be approximated by the orbital-based summation, similarly to how it is done in ref.[55] This results in the following expression:

$$E^{\mathrm{disp}}_{\mathrm{QM-EFP}} = -\frac{1}{\pi}\sum_{j\in B}\sum_{k}^{occ}\sum_{r}^{vir}\sum_{\alpha\beta}^{x,y,z}\langle k|T_\alpha^j|r\rangle\langle r|T_\beta^j|k\rangle \int_0^\infty \frac{\omega_{rk}^{\mathrm{A}}}{(\omega_{rk}^{\mathrm{A}})^2+\omega^2}\alpha_{\alpha\beta}^j(i\omega)\,d\omega \tag{17}$$

where ω_{rk}^A is the orbital energy difference between virtual orbital r and occupied orbital k of the QM region, j are points of fragment B where distributed polarizability tensors are located, and $\langle k|T_\alpha^j|r\rangle = -\int dr'\,k^*(r')\frac{(r'-R^j)_\alpha}{(|r'-R^j|)^3}r(r')$ are electric field integrals in the occupied-virtual block of the QM system.

eq 17 provides the dispersion interaction between the QM region (molecule A) and an effective fragment B. Summation over all fragments should be done to compute the total QM−EFP dispersion energy of the system. eq 17 requires the calculation of orbital energies and electric field integrals $\langle k|T_\alpha^j|r\rangle$ in the occupied-virtual block of the QM system. Effective fragments are still represented by distributed dynamic polarizability tensors. The imaginary frequency integral is evaluated similarly to the integral in the EFP−EFP energy expression, using the 12-point quadrature, as detailed in ref.[55] eq 17 is the working expression for the QM−EFP dispersion energy employed in this paper.

It is possible to further simplify eq 17 by introducing isotropic approximations for dynamic polarizabilities. First, setting off-diagonal terms of the polarizability tensors to zero, we define the diagonal approximation:

$$E^{\mathrm{disp,diag}}_{\mathrm{QM-EFP}} = -\frac{1}{\pi}\sum_{j\in B}\sum_{k}^{occ}\sum_{r}^{vir}\sum_{\beta}^{x,y,z}\langle k|T_\beta^j|r\rangle\langle r|T_\beta^j|k\rangle \int_0^\infty \frac{\omega_{rk}^{\mathrm{A}}}{(\omega_{rk}^{\mathrm{A}})^2+\omega^2}\alpha_{\beta\beta}^j(i\omega)\,d\omega \tag{18}$$

Additionally, application of a fully isotropic approximation, i.e., $\bar{\alpha} = \frac{1}{3}(\alpha_{xx}+\alpha_{yy}+\alpha_{zz})$, yields

$$E^{\mathrm{disp,iso}}_{\mathrm{QM-EFP}} = -\frac{1}{\pi}\sum_{j\in B}\sum_{k}^{occ}\sum_{r}^{vir}\sum_{\beta}^{x,y,z}\langle k|T_\beta^j|r\rangle\langle r|T_\beta^j|k\rangle \int_0^\infty \frac{\omega_{rk}^{\mathrm{A}}}{(\omega_{rk}^{\mathrm{A}})^2+\omega^2}\bar{\alpha}^j(i\omega)\,d\omega \tag{19}$$

The accuracy of these approximations will be discussed in the Results and Discussion section.

While the expression for the EFP−EFP dispersion energy eq 12 provides a clear separation into C_6 and R^{-6} parts, this separation is less obvious in eqs 17−19 for the QM−EFP dispersion. However, taking into account that the integral over the imaginary frequency range is distance-independent, it can be thought of as an effective C_6 coefficient. Then an approximate R^{-6} distance dependence should be contained in the product of integrals $\langle k|T_\alpha|r\rangle\langle r|T_\beta|k\rangle$. Even though the formal scaling of T_α is R^{-2}, a matrix element of an operator between occupied and virtual orbitals is analogous to the first variation of the operator that lowers the distance dependence of the property by R^{-1}. (Similarly, the second variation of the operator would lower the scaling by R^{-2}, as is the case in the MP2 energy expression, where matrix elements $\langle ij|\hat{V}|ab\rangle$

DOI: 10.1021/acs.jpca.7b05875
J. Phys. Chem. A 2017, 121, 9495−9507

asymptotically decay as R^{-3}, even though $\hat{V}$ has R^{-1} distance dependence.) As a result, the $\langle k|T_\alpha|r\rangle\langle r|T_\beta|k\rangle$ term provides the expected R^{-6} distance dependence for the dispersion energy. It should be noted that the orbital energies of the QM subsystem, and consequently the C_6 coefficients, will depend on the electrostatic (including Coulomb and polarization) interactions between the QM subsystem and all EFP fragments. This interesting phenomenon reflects the mixing of the dispersion and electrostatic interactions and will be discussed in the Results and Discussion section. Approximate molecular C_6 coefficients can be obtained by equating the computed dispersion energies from eq 17 to $E_6^{\text{disp}} = C_6 R^{-6}$, where R is the distance between the molecular centers of mass.

The formulation in eq 17 is along the same lines as the local response dispersion developed in the framework of time-dependent density functional theory (DFT) by Ikabata and Nakai.[56]

If one rewrites eq 17 as

$$E^{\text{disp}}_{\text{QM-EFP}} = -\frac{1}{\pi}\sum_{k}^{occ}\sum_{r}^{vir}\sum_{\alpha\beta}^{x,y,z}\frac{\langle k|T_\alpha|r\rangle\langle r|T_\beta|k\rangle}{\Delta^{kr}_{\alpha\beta}} \tag{20}$$

with denominator

$$\Delta^{kr}_{\alpha\beta} = \frac{1}{\int_0^\infty d\omega \frac{\omega^{\text{A}}_{rk}}{(\omega^{\text{A}}_{rk})^2+\omega^2}\alpha^{j\in\text{B}}_{\alpha\beta}(i\omega)} \tag{21}$$

there is a resemblance to the standard expression of second-order perturbation theory. Indeed, the denominator in eq 20 is proportional to the difference in orbital energies ω_{rk}, as becomes evident in the static approximation $i\omega \to 0$.

The computational algorithm for evaluating the QM−EFP dispersion energy is the following. The discussion below assumes that the EFP terms are computed by an EFP module and the ab initio computations are performed by an electronic structure software. The dispersion energy in the present implementation is an additive term that is computed after the SCF or Kohn−Sham equations for the QM subsystem are converged. The orbital energies of the QM subsystem are provided to the EFP module. An array of polarizability points, i.e., points at which the dynamic polarizability tensors of each fragment are located, is provided to the electronic structure package. For each of these points, electric field integrals are computed in the atomic orbital (AO) basis, converted to the molecular orbital (MO) basis, and the part corresponding to the occupied-virtual block (OCC × VIR) is transferred to the EFP module. At each polarizability point, the integral over the imaginary frequency range is evaluated for all occupied-virtual pairs, resulting in nine OCC x VIR arrays, based on the number of $(\alpha\beta)$ elements of a polarizability tensor. The (OCC,VIR) elements of these arrays are multiplied by the square of the corresponding elements of the electric field integrals, and the obtained numbers are summed over all occupied-virtual orbital pairs.

The computational cost of the dispersion energy calculation is associated with extracting the electric field integrals for a number of polarizability expansion points and contracting the occupied-virtual block of electric field integrals with the imaginary frequency integral. Overall, the cost of these computations is small to negligible compared to the cost of ab initio computations of the QM region.

The accuracy of eqs 17−19 is discussed in the Results and Discussion section. No short-range damping functions or scaling coefficients have been used, because the test results do not indicate a need for them. Future work involving molecular dynamics simulations of systems with strong H-bonding or ionic character might show that damping functions are required for stable simulations, in which case the damping functions can be introduced in a similar manner to how it is done for the EFP−EFP dispersion.

The QM−EFP dispersion energy term eq 17 is implemented in the *libefp* library;[57,58] fully functional codes exist in the Q-Chem[59]/*libefp* interface and in the GAMESS quantum chemistry package.[60,61]

An alternative implementation of the QM−EFP dispersion term was reported in ref 55. That implementation is more in the spirit of the EFP−EFP dispersion energy. In particular, eq 8 is considered as a starting point (i.e., a multipole expansion is employed both in the EFP and QM subsystems), but polarizability tensors are formed only for the EFP region, while dipole integrals are kept unchanged for the QM region. In an orbital-based approximation, this results in

$$E^{\text{disp}}_{\text{QM-EFP}} = -\frac{1}{\pi}\sum_{j\in B}\sum_{k}^{occ}\sum_{r}^{vir}\sum_{\alpha\beta\gamma\delta}^{x,y,z} T^{kj}_{\alpha\beta}T^{kj}_{\gamma\delta}\langle k|\hat{\mu}^{\text{A}}_\alpha|r\rangle\langle r|\hat{\mu}^{\text{A}}_\gamma|k\rangle \int_0^\infty \frac{\omega^{\text{A}}_{rk}}{(\omega^{\text{A}}_{rk})^2+\omega^2}\alpha^{j}_{\beta\delta}(i\omega)\,d\omega \tag{22}$$

While the general forms of eq 22 and eq 17 are quite similar, there are several important distinctions. Instead of the field integrals in eq 17, eq 22 operates with the dipole moment integrals $\langle k|\mu_\alpha|r\rangle$ in the occupied-virtual orbital block. Further, because the electronic coordinates of the QM subsystem are integrated out, there is no electronic coordinate present in eq 22, and the tensors T^{kj} operate on the distance R_{kj}, which is a radius vector between the centroid of orbital k of the QM subsystem and a distributed point j on fragment B. On the other hand, in eq 17, tensors T^j are computed between a fragment point j and an electron coordinate. In ref 55, polarizability tensors on fragments are approximated by isotropic component-averaged scalars, resulting in the expression

$$E^{\text{disp}}_{\text{QM-EFP}} = -\frac{6}{\pi}\sum_{j\in B}\sum_{k}^{occ}\sum_{r}^{vir}\frac{1}{R_{kj}^{\,6}}\langle k|\hat{\mu}^{\text{A}}|r\rangle\langle r|\hat{\mu}^{A}|k\rangle \int_0^\infty \frac{\omega^{\text{A}}_{rk}}{(\omega^{\text{A}}_{rk})^2+\omega^2}\bar{\alpha}^{j}(i\omega)\,d\omega \tag{23}$$

In order to ensure sufficient accuracy, expression 23 is further converted to the localized molecular orbital (LMO) basis. Similarly to the EFP−EFP dispersion, short-range damping functions as well as an empirical factor of $4/\pi$, that is intended to estimate higher-order even powers (e.g., C_8, C_{10}) dispersion terms are applied to ensure numerical accuracy. With these modifications, the final expression for the dispersion energy implemented in ref 55 is

$$E^{\text{disp}}_{\text{QM-EFP}} = -\frac{4}{3}\sum_{l\in QM}\sum_{\nu\in B}\frac{F_6^{l\nu}C_6^{l\nu}}{R_{l\nu}^{\,6}} \tag{24}$$

where l and ν are LMOs of the QM region and effective fragments, respectively, and the distance $R_{l\nu}$ is computed between centroids of localized orbitals l and ν. $F_6^{l\nu}$ is the damping function of one of two forms, Tang−Toennies based

DOI: 10.1021/acs.jpca.7b05875
J. Phys. Chem. A 2017, 121, 9495−9507

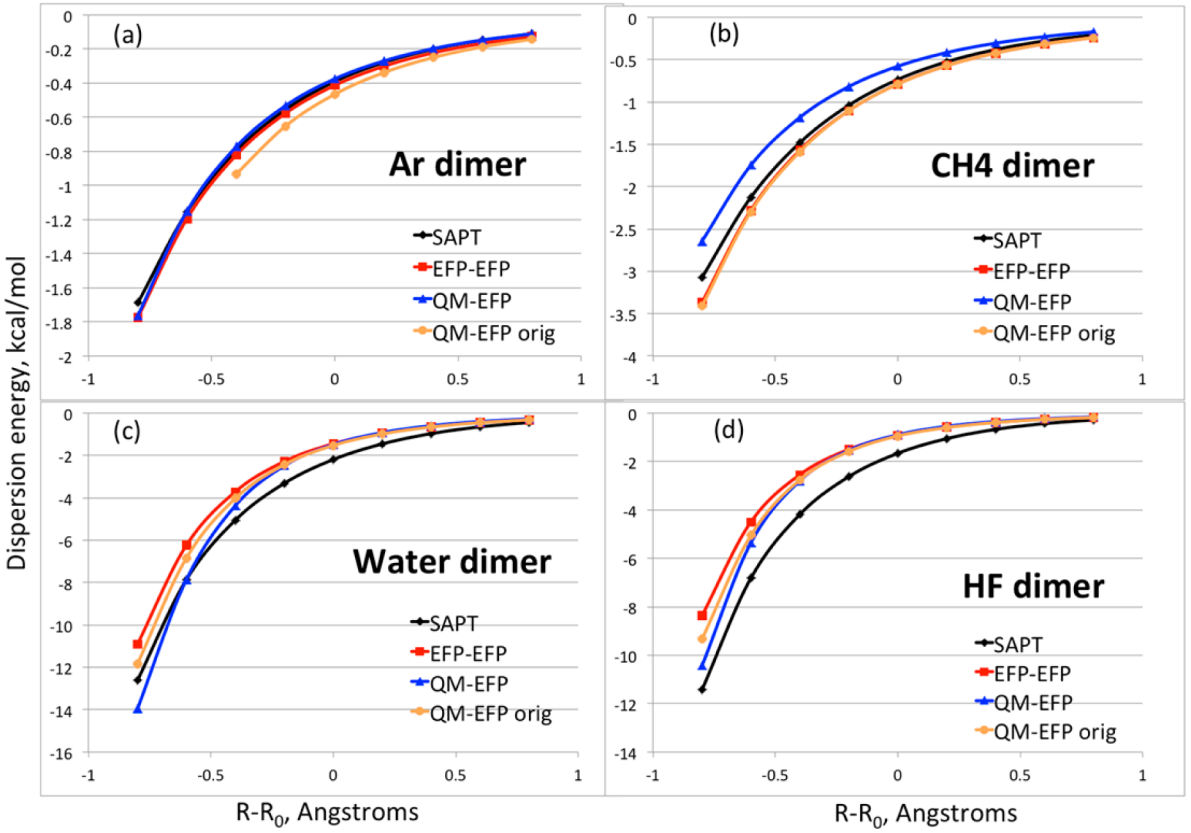

Figure 1. Dispersion energies (kcal/mol) in (a) Ar dimer, (b) methane dimer, (c) water dimer, and (d) HF dimer as a function of intermonomer separation computed using EFP−EFP (red squares), present QM−EFP (blue triangles), original QM−EFP data from ref 55 (orange circles), and SAPT2 (black diamonds).

or overlap-based, with the latter form being recommended.[55] The $C_6^{l\nu}$ coefficient between a pair of points l and ν has the following form:

$$C_6^{l\nu} = \frac{2}{\pi} \sum_{k}^{valence} \sum_{k'}^{valence} \sum_{\beta}^{x,y,z} L_{kl} \left[\sum_{r}^{vir} \langle k|\hat{\mu}_\beta|r\rangle\langle r|\hat{\mu}_\beta|k'\rangle \int_0^\infty \frac{\omega_{rk'}}{(\omega_{rk'})^2 + \omega^2} \bar{\alpha}^{\nu}(i\omega)\, d\omega \right] L_{k'l} \quad (25)$$

where localized $|l\rangle$ and canonical $|k\rangle$ ($|k'\rangle$) orbitals of the QM subsystem are related through the transformation matrix L_{kl}:

$$|l\rangle = \sum_k |k\rangle L_{kl} \quad (26)$$

The molecular C_6 coefficient can be obtained as a sum of contributions from all pairs of polarizability expansion points (LMO centroids) of molecules A and B.

While the formulations corresponding to eq 17 and eq 24 should provide comparable accuracy, there are several considerations that make using eq 17 more advantageous or computationally more efficient than eq 24. Expression 17 is more rigorous than expression 24 because it does not imply diagonal or isotropic approximations, even though eq 24 could also be reformulated without implying these approximations, similarly to how it is done for the R^{-7} and R^{-8} EFP−EFP dispersion terms.[54] The necessity of using orbital localization in the QM region is another concern of the formulation in eq 24. Orbital localization adds an additional computational cost that is dependent on the system size and the localization scheme. When modeling extended systems, configurational sampling often must be taken into account, which sets strict requirements on the computational efficiency of the method. While eq 17, which avoids the orbital localization step, is expected to be more tractable when sampling or dynamics simulations are performed, the use of localized orbitals is likely to result in more rapid convergence of the dispersion expansion in R^{-n}.

The analytic gradients of energy in eq 17 can be derived and implemented following the general strategy for gradients in the MP2 theory, using coupled perturbed Hartree−Fock equations.[62,63] This task will be accomplished in the near future. Analytic gradients based on eq 24 have been derived and are coded in GAMESS. The formulation of the dispersion energy between QM and EFP regions can be also extended to excited states, in the spirit of the CIS(D) method,[64] in which a dispersion correction will be computed perturbatively for each individual excited state.

3. COMPUTATIONAL DETAILS

A number of molecular systems were chosen for validation of the QM−EFP dispersion energy term. Unless stated otherwise, Hartree−Fock (HF) with the 6-311++G(3df,2p)[65−67] basis set was employed for the QM fragments. Symmetry adapted perturbation theory (SAPT)[68] has been used as a metric for evaluating the accuracy of the QM−EFP dispersion energy.

Several molecular dimers (Ar dimer, methane dimer, water dimer, HF dimer, sandwich and T-shaped configurations of the benzene dimer) have been considered at varying intermolecular separations. Geometries, EFP potentials and SAPT2 energy values (using the 6-311++G(3df,2p) basis set for Ar, methane,

DOI: 10.1021/acs.jpca.7b05875
J. Phys. Chem. A 2017, 121, 9495−9507

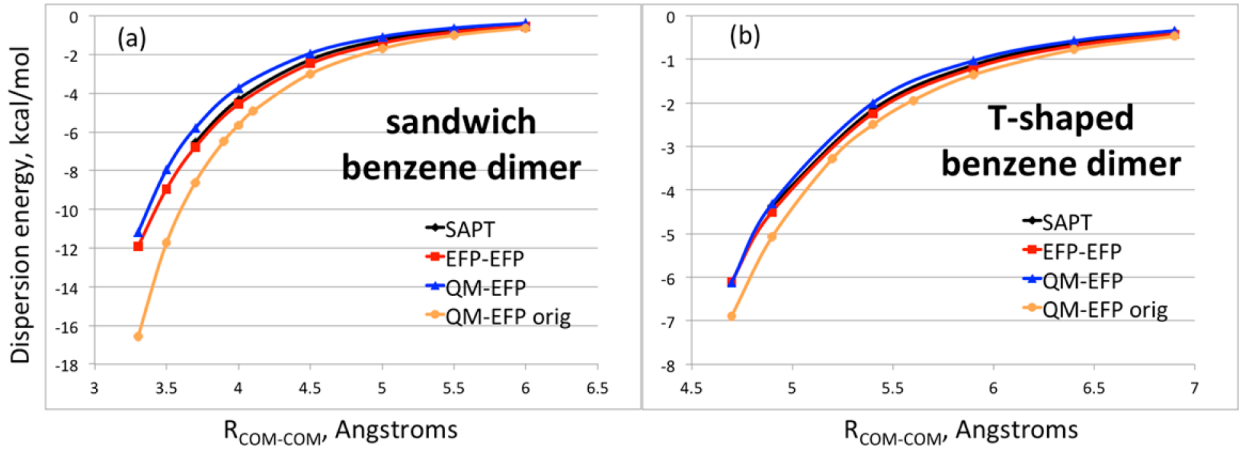

Figure 2. Dispersion energies (kcal/mol) in (a) sandwich and (b) T-shaped configurations of the benzene dimer as a function of the intermonomer separation computed using EFP−EFP (red squares), QM−EFP (blue triangles), QM−EFP data from ref 55 (orange circles), and SAPT2 (black diamonds).

water, and HF dimers, and the aug-cc-pVDZ basis set for the benzene dimers) were adapted from ref 31.

All dimers from the S22 data set were also considered.[69] Geometries and EFP potentials of those dimers are taken from ref 70.

Further, methanol dimer and methane dimer were computed with several basis sets employed for the QM monomer (6-31G(d), 6-31+G(d), 6-311G(d), 6-311+G(d), 6-311++G(d,p), 6-311++G(3df,2p), cc-pVDZ, aug-cc-pVDZ, cc-pVTZ, and aug-cc-pVTZ) with the HF reference, and 6-31+G(d) and 6-311++G(3df,2p) with the PBE0, BLYP, and B3LYP functionals. These calculations were performed at the equilibrium geometries of the methanol and methane dimers from ref 31; EFP potentials were taken from the same reference. While correlation-consistent basis sets are not optimized for HF calculations, it is important to test the accuracy of the dispersion energies computed in these commonly used basis sets.

The dispersion energies in the water-benzene dimer were computed at several intermonomer separations using the same EFP potentials as above. The equilibrium geometry is obtained from ref.[71] and displaced by 0.2, 0.4, −0.2, and −0.4 Å along a line connecting the center of mass of benzene and O atom of water. SAPT2+(3)/aug-cc-pVDZ calculations for this system were performed with the PSI4 electronic structure program.[72] SAPT2+(3) treats dispersion up to the second order in terms of intramonomer correlation as well as includes a third-order term for intermonomer correlation, i.e., $E_{\mathrm{disp}}^{\mathrm{SAPT2+(3)}} = E_{\mathrm{exch-disp}}^{(20)} + E_{\mathrm{disp}}^{(20)} + E_{\mathrm{disp}}^{(21)} + E_{\mathrm{disp}}^{(22)} + E_{\mathrm{disp}}^{(30)}$.

Finally, a local minimum of the water pentamer was considered, with the same EFP water potential used.

The geometries of all considered complexes can be found in the Supporting Information. All employed EFP potentials are stored online.[30]

4. RESULTS AND DISCUSSION

The goal of this section is to demonstrate the general accuracy of the QM−EFP dispersion energy implementation, with respect to the dispersion energy between two effective fragments (EFP−EFP) and from SAPT calculations. Several characteristic dimers of the dispersion-dominated bonding type (Ar, methane, and benzene dimers) and of the H-bonding type (water and HF dimers) are analyzed in detail. Further, the accuracy of the QM−EFP dispersion for the S22 data set of intermolecular interactions is assessed. Additionally, practical aspects of employing the QM−EFP dispersion term in electronic structure calculations is considered, as is its dependence on the basis set and density functional, as well as dependence on the electrostatic field of effective fragment(s). The relative accuracy of full anisotropic, diagonal, and isotropic approximations for the QM−EFP dispersion energy is examined.

Figure 1 compares the dispersion energies obtained with the new QM−EFP implementation (eq 17), the original QM−EFP formula[55] (eq 24), EFP−EFP interactions (eq 13) and SAPT2 for the Ar dimer, methane dimer, water dimer and HF dimer. Potential energy slices along a coordinate connecting the centers of masses in Ar and methane dimers, oxygen atoms in water dimer, and fluorine atoms in HF dimers are constructed, spanning a range of chemically relevant dimer geometries. Similar dispersion energy slices are shown in Figure 2 for two representative isomers of the benzene dimer, sandwich and T-shaped. In this case, absolute values of intermonomer separations (distances between benzene center of masses) are shown.

For all six considered dimers, there is generally good agreement between the QM−EFP dispersion energies and the EFP−EFP and SAPT values. The new QM−EFP dispersion curve closely matches the SAPT and EFP−EFP curves in the case of the Ar dimer and T-shaped benzene dimer. The new QM−EFP energies are underestimated with respect to both EFP−EFP and SAPT in the methane dimer and the sandwich benzene dimer. In water and HF dimers, both the original and the new QM−EFP and EFP−EFP energies agree with each other at equilibrium and long distances and start to deviate at shorter distances, with the new QM−EFP dispersion becoming more attractive. The more attractive behavior of the new QM−EFP dispersion at short intermonomer separations is attributed to missing short-range screening in the present QM−EFP formulation, while the EFP−EFP and original QM−EFP values are screened with the overlap-based damping functions. However, in all considered test cases, no examples have been found for which the missing short-range damping critically affects the accuracy or the stability of the calculation. The situation is quite different for the polarization energy, where

DOI: 10.1021/acs.jpca.7b05875
J. Phys. Chem. A 2017, 121, 9495−9507

short-range damping is essential due to the variational nature of the polarization energy term, to avoid polarization catastrophe.

Comparing the accuracy of the two QM−EFP dispersion implementations, it is noticeable in Figures 1 and 2 that the new formulation tends to slightly underestimate the dispersion energy in dispersion-dominated complexes (Ar, methane, benzene dimers) while the original QM−EFP implementation, as well as EFP−EFP dispersion, produces somewhat weaker dispersion in H-bonded dimers.

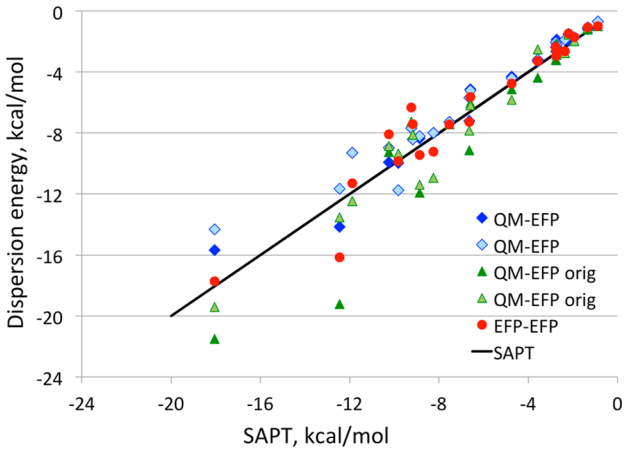

Figure 3. Dispersion energies (kcal/mol) in dimers of the S22 data set computed by EFP−EFP (red circles), QM−EFP with the first monomer treated quantum-mechanically (blue diamonds) and the second monomer treated quantum-mechanically (light blue diamonds), and original QM−EFP with the first monomer treated quantum-mechanically (green triangles) and the second monomer treated quantum-mechanically (light green triangles), compared to the SAPT2+(3)/aug-cc-pVTZ reference values.

Figure 3 and Table 1 provide further validation of the QM−EFP dispersion energy eq 17 by comparing dispersion energies obtained by different methods on the S22 data set of noncovalent interactions.[69] S22 is a database created to benchmark the accuracy of computational methods on a representative set of noncovalent dimers. S22 contains complexes of three types, H-bonded, dispersion-dominated, and mixed character. CCSD(T)/CBS reference energy values are available. Previously, the accuracy of EFP−EFP interactions was assessed, in which both monomers were represented by effective fragments.[70] In addition to comparing geometries and total interaction energies, the accuracy of the EFP energy components was analyzed, using SAPT2+(3)/aug-cc-pVTZ[73] as a reference method. In the present work the dispersion energy part of the same SAPT analysis is used to benchmark the original (eq 24) and new (eq 17) QM−EFP dispersion energies. EFP−EFP, QM−EFP, and SAPT dispersion energies for all dimers in S22 can be found in the Table S1 of Supporting Information.

Figure 3 presents a regression plot of the new and original QM−EFP and EFP−EFP dispersion energies with respect to the SAPT energies. Table 1 provides statistics on each method: mean signed and unsigned errors (MSE and MUE, respectively) and mean unsigned relative errors, i.e., a ratio of MUE to the average SAPT dispersion energy for a given set. As follows from Table 1, the new QM−EFP dispersion formula eq 17 performs similarly to the EFP−EFP dispersion, with the overall MUE being 0.82 kcal/mol for QM−EFP and 0.79 kcal/mol for EFP−EFP energies. However, there are also some noticeable differences. For example, the new QM−EFP dispersion energy almost always underestimates the SAPT dispersion energy, as follows from positive MSE values and similar overall MSE and MUE. In contrast, the EFP−EFP dispersion often overestimates the SAPT dispersion energies for dispersion-dominated complexes but underestimates SAPT dispersion energies for H-bonded ones. Also, the new QM−EFP dispersion is more accurate for H-bonded complexes, while EFP−EFP dispersion works better for dispersion-dominated and mixed-type dimers. As was already noticed in analysis of Figures 1 and 2, the original QM−EFP dispersion formulation underestimates dispersion energies in H-bonding complexes but overbinds dispersion-dominated and mixed complexes. On average, the original QM−EFP dispersion formula is slightly less accurate than the new QM−EFP formulation or EFP−EFP, with a total mean unsigned relative error of 16%.

Since the QM−EFP dispersion formula provides a different treatment of the polarizabilities of the QM and EFP parts, it is unsurprising that the dispersion energy in a nonsymmetric dimer would differ depending on which monomer is treated as a fragment and which one is treated as a quantum region. This phenomenon is clearly seen in Figure 3, where two QM−EFP values are shown for all dimers. The QM−EFP values are identical for homodimers in a symmetric orientation, e.g., formic acid dimer, benzene sandwich dimer, etc. In heterodimers or nonsymmetric homodimers, the discrepancies in dispersion energies can sometimes exceed 20%, with the worst cases observed being water dimer and benzene−indole dimers for the new QM−EFP formulation and benzene−HCN and benzene−indole for the original formula. For computing average values in Table 1, these QM−EFP dispersion energies were averaged.

Figure 4 demonstrates the basis set dependence of the QM−EFP dispersion energy for the methane dimer and methanol dimer. In these calculations, the same EFP potentials, i.e., the same basis set for computing the dynamic polarizability tensors

Table 1. Average Errors of New QM−EFP ("QM−EFP"), Original QM−EFP ("QM−EFP orig"), and EFP−EFP Dispersion Energies with Respect to SAPT2+(3)/aug-cc-pVTZ Values in the S22 Data Set[A]

	QM−EFP			QM−EFP orig			EFP		
	MSE	MUE	rel. error	MSE	MUE	rel. error	MSE	MUE	rel. error
H-bonded	0.43	0.73	0.10	0.76	0.77	0.11	1.12	1.13	0.16
dispersion	0.87	1.08	0.13	−1.63	1.67	0.20	−0.62	0.85	0.10
mixed	0.54	0.62	0.15	−0.22	0.71	0.18	0.20	0.38	0.09
all	0.63	0.82	0.13	−0.42	1.08	0.16	0.20	0.79	0.12

[A]Mean signed errors (MSE), mean unsigned errors (MUE), both in kcal/mol, and mean unsigned relative errors (rel. error) are shown.

DOI: 10.1021/acs.jpca.7b05875
J. Phys. Chem. A 2017, 121, 9495−9507

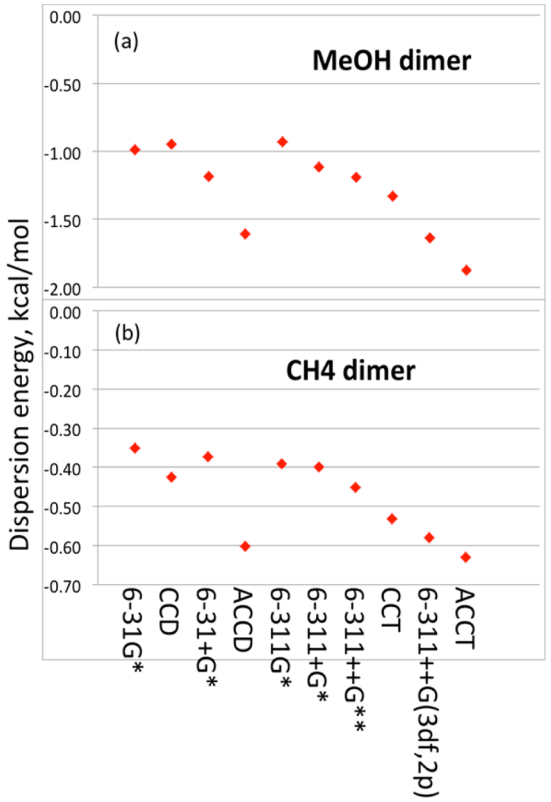

Figure 4. Basis set dependence of the QM−EFP dispersion energy (kcal/mol) in (a) methanol dimer and (b) methane dimer.

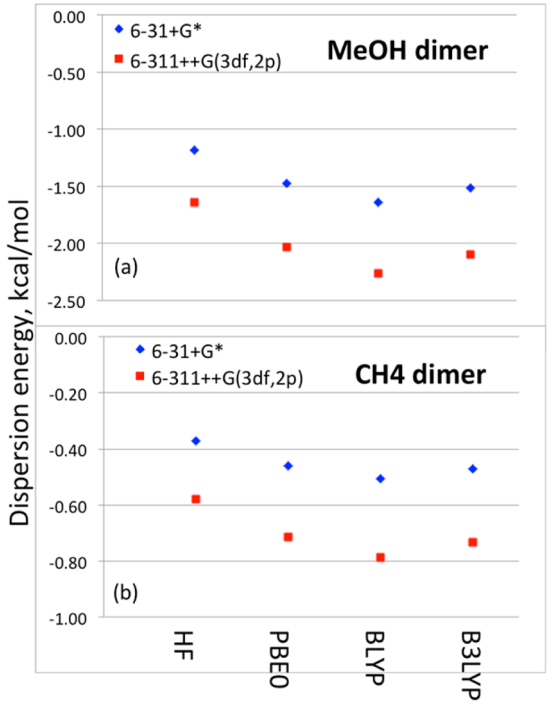

Figure 5. Dependence of the QM−EFP dispersion energy in (a) methanol dimer and (b) methane dimer on density functionals using the 6-31+G(d) (blue diamonds) and the 6-311++G(3df,2p) (red squares) basis sets.

of the fragments, are used throughout, but different basis sets for the QM molecule are tried. A strong basis set dependence of the dispersion energy, as for example is observed in SAPT, as well as in related molecular properties such as static and dynamic polarizabilities, is well-known.[74,75] Both dimers show a similar dependence of the dispersion energy on the basis set. The dispersion energy generally increases with an increase of ζ-level, i.e, from double-ζ to triple-ζ basis sets, and with adding polarization and, especially pronounced, diffuse functions. From the small double-ζ basis sets 6-31G(d) or cc-pVDZ to the large diffuse aug-cc-pVTZ basis set, the dispersion energy increases almost 2-fold. Note that the majority of the calculations in this work are performed with the 6-311++G(3df,2p) basis that provides close to convergence values of the dispersion term.

Given the popularity of Kohn−Sham (KS)-DFT for quantum-mechanical calculations, the dependence of the QM−EFP dispersion energy on various KS density functionals was explored. Figure 5 summarizes the values of the dispersion energy computed using two basis sets, 6-31+G(d) and 6-311++G(3df,2p), for Hartree−Fock (HF), BLYP, and the hybrid PBE0 and B3LYP functionals. As follows from Figure 5, all considered functionals result in larger (more attractive) values of the dispersion energies compared to that of Hartree−Fock. Hybrid functionals that contain a fraction of the Hartree−Fock exchange, PBE0 and B3LYP, have values that are in between those of HF and the nonhybrid functional BLYP. This trend is consistent for both basis sets and for the two different dimers. Generally, dispersion energies computed using DFT functionals are closer than HF to those predicted by SAPT2 calculations. For example, the SAPT dispersion energy of −0.74 kcal/mol in methane dimer[31] is right in the range of DFT predictions in the larger basis set (from −0.71 kcal/mol to −0.79 kcal/mol), and the DFT/6-311++G(3df,2p) dispersion energies in the methanol dimer (−2.03 to −2.26 kcal/mol) are in good agreement with the SAPT value of −2.25 kcal/mol.[31]

Figure 6 shows an interesting example of the dependence of the QM−EFP dispersion energies on fragment Coulomb and polarization fields. A water-benzene dimer is considered, in which the QM part (described at HF/6-311++G(3df,2p) level of theory) is either water (red curves) or benzene (blue curves). In this dimer, the water is a π-H bond donor. As was

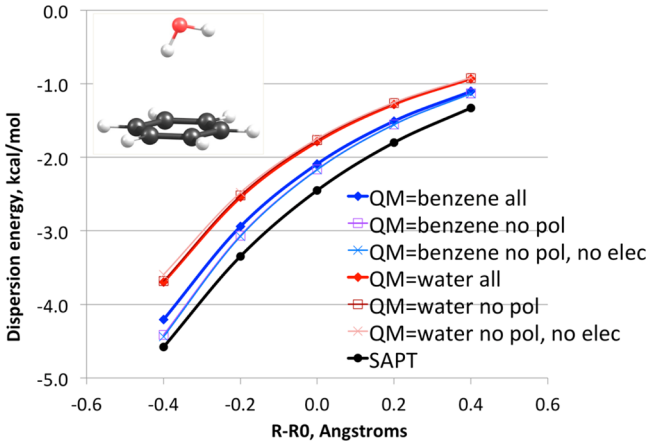

Figure 6. Electrostatic-dispersion coupling in water−benzene dimer. Black curve: SAPT2+(3)/aug-cc-pVDZ dispersion energy. Red curves: the water molecule is QM and the benzene is EFP. Blue curves: the benzene is QM and the water is EFP. Filled diamonds: the full effective fragment potential is used. Empty squares: the polarization term is turned off. Crosses: both electrostatic and polarization terms are turned off.

DOI: 10.1021/acs.jpca.7b05875
J. Phys. Chem. A 2017, 121, 9495−9507

already discussed above, due to a different treatment of the polarizabilities of the QM and EFP regions, the dispersion energy in a nonsymmetric dimer such as the water-benzene system differs depending on which monomer is treated as a fragment and which one is treated as a quantum region. This difference amounts to ~0.3 kcal/mol at the equilibrium separation. A scenario in which benzene represents a QM subsystem and water is an EFP fragment, provides better agreement with SAPT2+(3)/aug-cc-pVDZ results. When the benzene molecule is described quantum-mechanically, the Coulomb and polarization energy terms produce a slight decrease in the magnitude of the dispersion energy. Interestingly, the main destabilizing effect comes from the polarization, as can be seen by comparing the curve with turned-off polarization against the curve with turned-off polarization and Coulomb terms. The coupling of the Coulomb−polarization interaction with dispersion increases at shorter interfragment distances, constituting around 5% of the dispersion energy at a distance that is 0.4 Å shorter than the equilibrium distance. As expected, the dependence of the dispersion on the electrostatic field is weaker when the benzene molecule is the effective fragment (red curves), and in this case the main effect arises due to the Coulomb rather than the polarization term. Despite a small change in the dispersion energy in the case of the quantum water, it is interesting to note that the shift is in the opposite direction to what was observed in the case of the quantum benzene; i.e., electrostatic interactions stabilize the dispersion energy.

The coupling between the Coulomb−polarization and dispersion terms in QM−EFP comes from changes in the shapes and energies of the molecular orbitals of the QM region due to Coulomb and polarization interactions with effective fragment(s). It should be noted that this coupling is nonpairwise, as the combined electrostatic field of all fragments that are present affects the electronic wave function and the dispersion interactions with each individual fragment. Of course, the Coulomb and polarization interactions are naturally coupled with the dispersion in fully quantum calculations. However, there is no one-to-one correspondence between polarization-dispersion couplings observed in this QM−EFP model and higher-order couplings in SAPT theory such as $E^{30}_{\mathrm{ind-disp}}$ term, partly because in the QM−EFP model only the QM region is affected by the field of EFP fragments, while no changes in dynamic polarizabilities of fragments occur due to interactions with other fragments or QM region.

Figure 7 and Table 2 further illustrate the interdependence between dispersion and electrostatic interactions. A local minimum of the water pentamer is considered, in which a central water molecule builds four H-bonds with peripheral waters. The central water is always treated quantum-mechanically, while all other waters are effective fragments. Waters 2 and 3 are H-bond donors to the central water; waters 1 and 4 are H-bond acceptors to the central water. The QM water - four EFP waters system incudes data for all QM−EFP pair interactions as well.

The numbering on the plot of Figure 7 corresponds to the water numbers shown on the scheme of the water cluster. SAPT2+(3)/aug-cc-pVDZ data are also shown for reference. In calculations of the pentamer, SAPT calculations included two fragments: one containing a central water, and the other one containing four remaining waters. As with other examples, QM−EFP dispersion is in qualitative agreement with the SAPT data. It is evident from Figure 7 and Table 2 that the

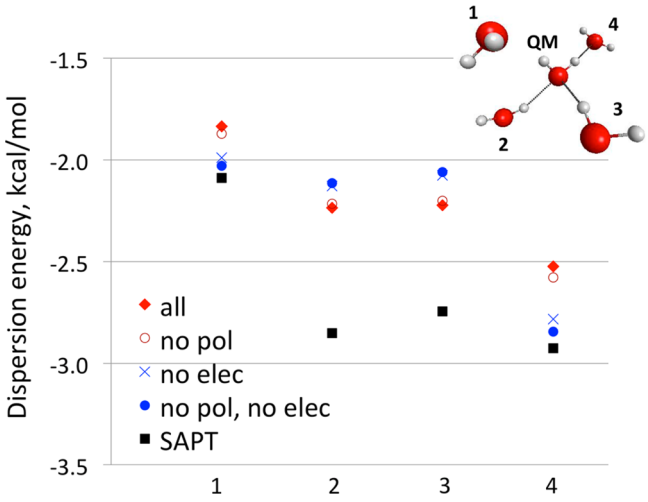

Figure 7. Electrostatic-dispersion coupling in water pentamer. The central water is QM, while the other waters are represented by effective fragments. Dispersion energies for each pair (one QM water and one EFP water, numbering in the graph corresponds to numbering in the molecular cluster) are plotted. EFP potentials with electrostatic and polarization terms (red diamonds), with turned off polarization (empty red circles), without electrostatics (blue crosses), and without polarization and electrostatic terms (blue circles) are considered. SAPT2+(3)/aug-cc-pVDZ data are shown with black squares.

electrostatic fields of the H-donors and H-acceptors shift dispersion energies in opposite directions. Specifically, the field of EFP H-donors (molecules 2 and 3) increases dispersion, while the field of EFP H-acceptors (molecules 1 and 4) diminishes the magnitude of the dispersion. In all cases, most of the effect arises due to the electrostatic term; the polarization plays a minor role. The observed values of the couplings are quite substantial and exceed 10% of the dispersion contribution for the EFP H-bond acceptors.

Table 2 summarizes the many-body nature of the electrostatic-dispersion coupling. Specifically, the sum of the dimer dispersion contributions differs from the total dispersion energy of the pentamer (one QM and four EFP waters). The many-body effect is small, on the order of 1% of the total dispersion energy, and is dominated by the electrostatic terms. Another important observation is that the electrostatic-dispersion coupling somewhat cancels out in the water pentamer and constitutes only 3% (to be compared with ~10% values of coupling in the dimers). This observation suggests that the couplings might be more significant in nonhomogeneous environments such as interfaces and less important in a homogeneous bulk environment.

Returning to the question of the origin of the electrostatic-dispersion coupling, one can consider two effects (see eq 17): changes in the electric field integrals $\langle k|T_\alpha|r\rangle$ and changes in the orbital energies due to the electrostatic field of the fragments. The values of the dispersion energies are quadratically dependent on the field integrals and approximately inversely proportional to the orbital energy differences ω^A_{rk}. Alternatively, exploring eq 23, where transition dipoles are introduced, dispersion energies are proportional to

$$E^{\mathrm{disp}}_{\mathrm{QM-EFP}} \sim \sum_k^{occ}\sum_r^{vir} \frac{\langle k|\mu|r\rangle\langle r|\mu|k\rangle}{\omega_{kr}} \sim \sum_k^{occ}\sum_r^{vir} \frac{f_{kr}}{(\omega_{kr})^2} \qquad (27)$$

DOI: 10.1021/acs.jpca.7b05875
J. Phys. Chem. A 2017, 121, 9495−9507

Table 2. Many-Body Nature of the Electrostatic-Dispersion Coupling[a]

	all	no pol	no elec	no pol, no elec	SAPT
dimer, EFP water 1	−1.835	−1.872	−1.990	−2.030	−2.089
dimer, EFP water 2	−2.235	−2.216	−2.128	−2.115	−2.852
dimer, EFP water 3	−2.224	−2.202	−2.075	−2.061	−2.744
dimer, EFP water 4	−2.523	−2.579	−2.784	−2.845	−2.926
dimer sum[b]	−8.817	−8.868	−8.977	−9.051	−10.611
pentamer, EFP waters 1, 2, 3, 4	−8.747	−8.789	−8.982	−9.051	−10.624
many-body effect[c]	0.070	0.079	−0.005	0.000	−0.013

[a]QM−EFP dispersion energies (kcal/mol) of the water pentamer system with different variants of EFP potentials ("all": all terms present; "no pol": polarization is turned off; "no elec": electrostatics is turned off; "no pol, no elec": polarization and electrostatics are turned off) are shown. SAPT corresponds to SAPT2+(3)/aug-cc-pVDZ calculations. [b]Sum of the dimer dispersion energies (rows 1−4). [c]Difference of the dispersion energies in the pentamer and all dimers.

where f_{kr} is the oscillator strength of the electronic transition between orbitals k and r. Thus, qualitatively, the dispersion energy is proportional to the sum of the oscillator strengths of all single-electron transitions in the system. The latter expression can be used to semiqualitatively predict changes in the dispersion energy due to electrostatic effects based on understanding how specific interactions between QM and EFP subsystems affect oscillator strengths of low-lying bright electronic excited states.

Finally, consider the importance of including off-diagonal terms in the dynamic polarizability tensors in eq 17. Table 3 compares the numerical values obtained by using eq 17 (all tensor terms are included), eq 18 (off-diagonal terms of polarizability tensors are ignored), and eq 19 (isotropic approximation, average values of the polarizability tensors are used). Analysis of Table 3 reveals that the diagonal approximation introduces only a minor error (within 2%) to the dispersion energy values. Thus, the diagonal approximation can be safely used in practice. However, the isotropic approximation provides a more significant effect, especially for the complexes dominated by H-bonding such as water and HF dimers. Since the errors introduced by the isotropic approximation can be of both signs (i.e., either improving or decreasing accuracy of the QM−EFP dispersion energies with respect to the SAPT values), using the isotropic approximation is not recommended. Deviations between full, diagonal and isotropic values increase insignificantly (in percentage values) at shorter intermolecular separations.

Table 3. QM−EFP Dispersion Energies (kcal/mol) at Equilibrium Separation between the Monomers Using Full Dynamic Polarizability Tensors as in Eq 17 and Diagonal (Eq 18) or Isotropic (Eq 19) Approximations[a]

	full	diagonal	isotropic
methane dimer	−0.58	−0.59 (2.4%)	−0.61 (5.3%)
Ar dimer	−0.37	−0.37 (−0.9%)	−0.35 (−6.8%)
water dimer	−1.48	−1.46 (−1.1%)	−1.24 (−15.9%)
HF dimer	−0.90	−0.88 (−1.4%)	−0.74 (−17.4%)
benzene sandwich dimer	−5.80	−5.81 (0.1%)	−6.30 (8.6%)
benzene T-shaped dimer	−4.31	−4.28 (−0.7%)	−4.60 (6.7%)

[a]Values in parentheses are percent errors with respect to the full dispersion energy computations.

5. CONCLUSIONS

A new formulation of the dispersion energy between quantum-mechanical and classical (represented by the effective fragments) subsystems is presented. Computation of the dispersion energies involves the evaluation of the electric field integrals in the occupied-virtual molecular orbital block of the QM region at the points where the polarizability tensors of the effective fragments are located. Dynamic polarizability tensors obtained from preparatory quantum mechanical calculations on each fragment is the only information required from the EFP subsystem. The computational cost of computing the dispersion energy is negligible compared to the cost of solving Hartree−Fock or Kohn−Sham equations for the QM subsystem. The dispersion energy is an additive contribution to the total energy of the QM−EFP system.

Numerical tests demonstrate that the accuracy of the QM−EFP dispersion energy is comparable to the accuracy of the EFP−EFP dispersion term. Thus, the new term preserves the present accuracy of the EFP method. The dispersion energy can be computed based on either Hartree−Fock or Kohn−Sham solutions of the QM subsystem, the latter providing somewhat larger values of the dispersion energies. Employing a larger or more diffuse basis set in the QM region will also increase the magnitude of the dispersion term. As the QM−EFP dispersion is treated quantum-mechanically, coupling between electrostatic/polarization and dispersion terms arises. This is because the electrostatic field of the fragments modifies the electronic wave function of the QM system, thus affecting the values of the integrals and orbital energies entering the expression of the dispersion energy. The electrostatic-dispersion coupling might be significant when the solute experiences strong electrostatic fields due to a nonhomogeneous environment, as is often observed at interfaces, but is expected to be less noticeable in nonpolar solvents and in homogeneous surroundings.

While the implementation of the dispersion energy presented here involves anisotropic distributed dynamic polarizability tensors on the effective fragments, it is safe to ignore off-diagonal terms and use diagonal dynamic polarizability tensors. However, using a fully isotropic approximation is not recommended as it results in significant and nonsystematic deviations.

Development of the QM−EFP dispersion energy term contributes to the development of the embedded QM/EFP models for describing electronic processes in condensed phases, with full quantum-mechanical coupling between QM and EFP subsystems. Future work will include extensions of the QM−EFP dispersion energy term to open-shell systems and electronic excited states, as well as the development of the analytic gradients.

DOI: 10.1021/acs.jpca.7b05875
J. Phys. Chem. A 2017, 121, 9495−9507

■ ASSOCIATED CONTENT

Supporting Information

The Supporting Information is available free of charge on the ACS Publications website at DOI: 10.1021/acs.jpca.7b05875.

Structural data of molecular complexes considered in this work and QM−EFP, EFP and SAPT energies of S22 complexes (PDF)

■ AUTHOR INFORMATION

Corresponding Author

*(L.V.S.) E-mail: lslipchenko@purdue.edu.

ORCID

Lyudmila V. Slipchenko: 0000-0002-0445-2990
Mark S. Gordon: 0000-0001-6893-553X
Klaus Ruedenberg: 0000-0003-4834-0314

Notes

The authors declare no competing financial interest.

■ ACKNOWLEDGMENTS

L.V.S. acknowledges support of the National Science Foundation (Grants CHE-1465154 and CHE-1450088). M.S.G. acknowledges the support of National Science Foundation Grant CHE-1450217. Discussions with Drs. Emilie Guidez and Peng Xu are gratefully acknowledged.

■ REFERENCES

(1) Gordon, M. S.; Fedorov, D. G.; Pruitt, S. R.; Slipchenko, L. V. Fragmentation Methods: A Route to Accurate Calculations on Large Systems. *Chem. Rev.* **2012**, *112*, 632−672.

(2) Senn, H. M.; Thiel, W. QM/MM Methods for Biomolecular Systems. *Angew. Chem., Int. Ed.* **2009**, *48*, 1198−1229.

(3) Friesner, R. A.; Guallar, V. Ab Initio Quantum Chemical and Mixed Quantum Mechanics/Molecular Mechanics (QM/MM) Methods for Studying Enzymatic Catalysis. *Annu. Rev. Phys. Chem.* **2005**, *56*, 389−427.

(4) Becke, A. D.; Johnson, E. R. Exchange-Hole Dipole Moment and the Dispersion Interaction Revisited. *J. Chem. Phys.* **2007**, *127*, 154108.

(5) Grimme, S.; Antony, J.; Ehrlich, S.; Krieg, H. A Consistent and Accurate Ab Initio Parametrization of Density Functional Dispersion Correction (DFT-D) for the 94 Elements H-Pu. *J. Chem. Phys.* **2010**, *132*, 154104.

(6) Burns, L. A.; Mayagoitia, Á. V.; Sumpter, B. G.; Sherrill, C. D. Density-Functional Approaches to Noncovalent Interactions: A Comparison of Dispersion Corrections (DFT-D), Exchange-Hole Dipole Moment (XDM) Theory, and Specialized Functionals. *J. Chem. Phys.* **2011**, *134*, 084107.

(7) Tkatchenko, A.; Scheffler, M. Accurate Molecular Van Der Waals Interactions from Ground-State Electron Density and Free-Atom Reference Data. *Phys. Rev. Lett.* **2009**, *102*, 073005.

(8) Tkatchenko, A.; DiStasio, R. A.; Car, R.; Scheffler, M. Accurate and Efficient Method for Many-Body Van Der Waals Interactions. *Phys. Rev. Lett.* **2012**, *108*, 236402.

(9) Wesolowski, T. A. Embedding Potentials for Excited States of Embedded Species. *J. Chem. Phys.* **2014**, *140*, 18A530.

(10) Khait, Y. G.; Hoffmann, M. R. Embedding Theory for Excited States. *J. Chem. Phys.* **2010**, *133*, 044107.

(11) Schwabe, T.; Olsen, J. g. M. H.; Sneskov, K.; Kongsted, J.; Christiansen, O. Solvation Effects on Electronic Transitions: Exploring the Performance of Advanced Solvent Potentials in Polarizable Embedding Calculations. *J. Chem. Theory Comput.* **2011**, *7*, 2209−2217.

(12) Chai, J.-D.; Head-Gordon, M. Long-Range Corrected Hybrid Density Functionals with Damped Atom-Atom Dispersion Corrections. *Phys. Chem. Chem. Phys.* **2008**, *10*, 6615−6620.

(13) Lao, K. U.; Herbert, J. M. Accurate Intermolecular Interactions at Dramatically Reduced Cost: XPol+SAPT with Empirical Dispersion. *J. Phys. Chem. Lett.* **2012**, *3*, 3241−3248.

(14) Xie, W.; Gao, J. Design of a Next Generation Force Field: The X-Pol Potential. *J. Chem. Theory Comput.* **2007**, *3*, 1890−1900.

(15) Fedorov, D. G.; Kitaura, K. Extending the Power of Quantum Chemistry to Large Systems with the Fragment Molecular Orbital Method. *J. Phys. Chem. A* **2007**, *111*, 6904−6914.

(16) Steinmann, C.; Fedorov, D. G.; Jensen, J. H. Effective Fragment Molecular Orbital Method: A Merger of the Effective Fragment Potential and Fragment Molecular Orbital Methods. *J. Phys. Chem. A* **2010**, *114*, 8705−8712.

(17) Pomogaeva, A.; Chipman, D. M. New Implicit Solvation Models for Dispersion and Exchange Energies. *J. Phys. Chem. A* **2013**, *117*, 5812−5820.

(18) Piecuch, P. Spherical Tensor Theory of Long-Range Interactions in a System of N Arbitrary Molecules Including Quantum-Mechanical Many-Body Effects. *Mol. Phys.* **1986**, *59*, 1085−1095.

(19) Gordon, M. S.; Freitag, M. A.; Bandyopadhyay, P.; Jensen, J. H.; Kairys, V.; Stevens, W. J. The Effective Fragment Potential Method: A QM-Based MM Approach to Modeling Environmental Effects in Chemistry. *J. Phys. Chem. A* **2001**, *105*, 293−307.

(20) Gordon, M. S.; Slipchenko, L. V.; Li, H.; Jensen, J. H. The Effective Fragment Potential: A General Method for Predicting Intermolecular Forces. *Annu. Rep. Comput. Chem.* **2007**, *3*, 177−193.

(21) Ghosh, D.; Kosenkov, D.; Vanovschi, V.; Williams, C. F.; Herbert, J. M.; Gordon, M. S.; Schmidt, M. W.; Slipchenko, L. V.; Krylov, A. I. Noncovalent Interactions in Extended Systems Described by the Effective Fragment Potential Method: Theory and Application to Nucleobase Oligomers. *J. Phys. Chem. A* **2010**, *114*, 12739−12754.

(22) Gordon, M. S.; Smith, Q. A.; Xu, P.; Slipchenko, L. V. Accurate First Principles Model Potentials for Intermolecular Interactions. *Annu. Rev. Phys. Chem.* **2013**, *64*, 553−578.

(23) Ghosh, D.; Kosenkov, D.; Vanovschi, V.; Flick, J.; Kaliman, I.; Shao, Y.; Gilbert, A. T. B.; Krylov, A. I.; Slipchenko, L. V. Effective Fragment Potential Method in Q-Chem: A Guide for Users and Developers. *J. Comput. Chem.* **2013**, *34*, 1060−1070.

(24) Ponder, J. W.; Wu, C.; Ren, P.; Pande, V. S.; Chodera, J. D.; Schnieders, M. J.; Haque, I.; Mobley, D. L.; Lambrecht, D. S.; DiStasio, R. A.; et al. Current Status of the Amoeba Polarizable Force Field. *J. Phys. Chem. B* **2010**, *114*, 2549−2564.

(25) Piquemal, J. P.; Cisneros, G. A.; Reinhardt, P.; Gresh, N.; Darden, T. A. Towards a Force Field Based on Density Fitting. *J. Chem. Phys.* **2006**, *124*, 104101.

(26) Cisneros, G. A.; Darden, T. A.; Gresh, N.; Pilmé, J.; Reinhardt, P.; Parisel, O.; Piquemal, J. P. Design of Next Generation Force Fields from Ab Initio Computations: Beyond Point Charges Electrostatics. *Multi-Scale Quantum Models for Biocatalysis* **2009**, *7*, 137−172.

(27) Steindal, A. H.; Ruud, K.; Frediani, L.; Aidas, K.; Kongsted, J. Excitation Energies in Solution: The Fully Polarizable QM/MM/PCM Method. *J. Phys. Chem. B* **2011**, *115*, 3027−3037.

(28) Grimme, S. A General Quantum Mechanically Derived Force Field (Qmdff) for Molecules and Condensed Phase Simulations. *J. Chem. Theory Comput.* **2014**, *10*, 4497−514.

(29) McDaniel, J. G.; Yu, K.; Schmidt, J. R. Ab Initio, Physically Motivated Force Fields for Co2 Adsorption in Zeolitic Imidazolate Frameworks. *J. Phys. Chem. C* **2012**, *116*, 1892−1903.

(30) Slipchenko, L. V. EFP Fragment Library. https://github.com/makefp/EFP_potentials.

(31) Slipchenko, L. V.; Gordon, M. S. Damping Functions in the Effective Fragment Potential Method. *Mol. Phys.* **2009**, *107*, 999−1016.

(32) Chen, J. H.; Martinez, T. J. Qtpie: Charge Transfer with Polarization Current Equalization. A Fluctuating Charge Model with Correct Asymptotics. *Chem. Phys. Lett.* **2007**, *438*, 315−320.

(33) Damjanovic, A.; Kosztin, I.; Kleinekathöfer, U.; Schulten, K. Excitons in a Photosynthetic Light-Harvesting System: A Combined Molecular Dynamics, Quantum Chemistry, and Polaron Model Study.

DOI: 10.1021/acs.jpca.7b05875
J. Phys. Chem. A 2017, 121, 9495−9507

Phys. Rev. E: Stat. Phys., Plasmas, Fluids, Relat. Interdiscip. Top. **2002**, *65*, 031919.
(34) Froese, R. D. J.; Morokuma, K. The Imomo and Imonm Methods for Excited States. A Study of the Adiabatic S0–> T1,2 Excitation Energies of Cyclic Alkenes and Enones. *Chem. Phys. Lett.* **1996**, *263*, 393−400.
(35) Gao, J. Hybrid Quantum and Molecular Mechanical Simulations: An Alternative Avenue to Solvent Effects in Organic Chemistry. *Acc. Chem. Res.* **1996**, *29*, 298−305.
(36) Gao, J. Methods and Applications of Combined Quantum Mechanical and Molecular Mechanical Potentials. *Rev. Comput. Chem.* **1996**, *7*, 119.
(37) Gao, J.; Truhlar, D. G. Quantum Mechanical Methods for Enzyme Kinetics. *Annu. Rev. Phys. Chem.* **2002**, *53*, 467−505.
(38) Field, M. J.; Bash, P. A.; Karplus, M. Combined Quantum Mechanical and Molecular Mechanical Potential for Molecular Dynamics Simulations. *J. Comput. Chem.* **1990**, *11*, 700−733.
(39) Mordasini, T. Z.; Thiel, W. Combined Quantum Mechanical and Molecular Mechanical Approaches. *Chimia* **1998**, *52*, 288−291.
(40) Singh, U. C.; Kollman, P. A. Combined Ab Initio Quantum Mechanical and Molecular Mechanical Method for Carrying out Simulations on Complex Molecular Systems: Applications to the Ch3cl + Cl Exchange Reaction and Gas Phase Protonation of Polyethers. *J. Comput. Chem.* **1986**, *7*, 718−730.
(41) Stanton, R. V.; Little, L. R.; Merz, K. M. An Examination of a Hartree-Fock/Molecular Mechanical Coupled Potential. *J. Phys. Chem.* **1995**, *99*, 17344−17348.
(42) Warshel, A.; Levitt, M. Theoretical Studies of Enzymic Reactions: Dielectric, Electrostatic and Steric Stabilization of the Carbonium Ion in the Reaction of Lysozyme. *J. Mol. Biol.* **1976**, *103*, 227−249.
(43) Canfield, P.; Dahlbom, M. G.; Hush, N. S.; Reimers, J. R. Density-Functional Geometry Optimization of the 150 000-Atom Photosystem-I Trimer. *J. Chem. Phys.* **2006**, *124*, 024301−15.
(44) Svensson, M.; Humbel, S.; Froese, R. D. J.; Matsubara, T.; Sieber, S.; Morokuma, K. Oniom: A Multilayered Integrated MO + MM Method for Geometry Optimizations and Single Point Energy Predictions. A Test for Diels-Alder Reactions and Pt(P(T-Bu)3)2 + H2 Oxidative Addition. *J. Phys. Chem.* **1996**, *100*, 19357−19363.
(45) Vreven, T.; Morokuma, K.; Farkas, O.; Schlegel, H. B.; Frisch, M. J. Geometry Optimization with Qm/Mm, Oniom, and Other Combined Methods. I. Microiterations and Constraints. *J. Comput. Chem.* **2003**, *24*, 760−769.
(46) Higashi, M.; Truhlar, D. G. Combined Electrostatically Embedded Multiconfiguration Molecular Mechanics and Molecular Mechanical Method: Application to Molecular Dynamics Simulation of a Chemical Reaction in Aqueous Solution with Hybrid Density Functional Theory. *J. Chem. Theory Comput.* **2008**, *4*, 1032−1039.
(47) Tishchenko, O.; Truhlar, D. G. Non-Hermitian Multiconfiguration Molecular Mechanics. *J. Chem. Theory Comput.* **2009**, *5*, 1454−1461.
(48) Arul Murugan, N.; Kongsted, J.; Rinkevicius, Z.; Aidas, K.; Ågren, H. Modeling the Structure and Absorption Spectra of Stilbazolium Merocyanine in Polar and Nonpolar Solvents Using Hybrid Qm/Mm Techniques. *J. Phys. Chem. B* **2010**, *114*, 13349−13357.
(49) Ma, H.; Ma, Y. Solvatochromic Shifts of Polar and Non-Polar Molecules in Ambient and Supercritical Water: A Sequential Quantum Mechanics/Molecular Mechanics Study Including Solute-Solvent Electron Exchange-Correlation. *J. Chem. Phys.* **2012**, *137*, 214504.
(50) Stone, A. J. *The Theory of Intermolecular Forces*. Oxford University Press: Oxford, U.K., 1996.
(51) McLachlan, A. D. Retarded Dispersion Forces between Molecules. *Proc. R. Soc. London, Ser. A* **1963**, *271*, 387−401.
(52) Adamovic, I.; Gordon, M. S. Dynamic Polarizability, Dispersion Coefficient C6 and Dispersion Energy in the Effective Fragment Potential Method. *Mol. Phys.* **2005**, *103*, 379−387.
(53) Guidez, E. B.; Gordon, M. S. Dispersion Correction Derived from First Principles for Density Functional Theory and Hartree−Fock Theory. *J. Phys. Chem. A* **2015**, *119*, 2161−2168.
(54) Xu, P.; Zahariev, F.; Gordon, M. S. The R^{-7} Dispersion Interaction in the General Effective Fragment Potential Method. *J. Chem. Theory Comput.* **2014**, *10*, 1576−1587.
(55) Smith, Q. A.; Ruedenberg, K.; Gordon, M. S.; Slipchenko, L. V. The Dispersion Interaction between Quantum Mechanics and Effective Fragment Potential Molecules. *J. Chem. Phys.* **2012**, *136*, 244107.
(56) Ikabata, Y.; Nakai, H. Extension of Local Response Dispersion Method to Excited-State Calculation Based on Time-Dependent Density Functional Theory. *J. Chem. Phys.* **2012**, *137*, 124106.
(57) Kaliman, I. A.; Slipchenko, L. V. Libefp: A New Parallel Implementation of the Effective Fragment Potential Method as a Portable Software Library. *J. Comput. Chem.* **2013**, *34*, 2284−2292.
(58) Kaliman, I. A.; Slipchenko, L. V. Hybrid MPI/OpenMP Parallelization of the Effective Fragment Potential Method in the Libefp Software Library. *J. Comput. Chem.* **2015**, *36*, 129−135.
(59) Shao, Y.; Gan, Z.; Epifanovsky, E.; Gilbert, A. T. B.; Wormit, M.; Kussmann, J.; Lange, A. W.; Behn, A.; Deng, J.; Feng, X.; et al. Advances in Molecular Quantum Chemistry Contained in the Q-Chem 4 Program Package. *Mol. Phys.* **2015**, *113*, 184−215.
(60) Schmidt, M. W.; Baldridge, K. K.; Boatz, J. A.; Elbert, S. T.; Gordon, M. S.; Jensen, J. H.; Koseki, S.; Matsunaga, N.; Nguyen, K. A.; Su, S. J.; et al. General Atomic and Molecular Electronic-Structure System. *J. Comput. Chem.* **1993**, *14*, 1347−1363.
(61) Gordon, M. S.; Schmidt, M. W. Advances in Electronic Structure Theory: Gamess a Decade Later. In *Theory and Applications of Computational Chemistry*; Dykstra, C. E., Frenking, G., Kim, K. S., Scuseria, G. E., Eds.; Elsevier: 2005; pp 1167−1190.
(62) Pople, J. A.; Krishnan, R.; Schlegel, H. B.; Binkley, J. S. Derivative Studies in Hartree-Fock and Møller-Plesset Theories. *Int. J. Quantum Chem.* **1979**, *16*, 225−241.
(63) Frisch, M. J.; Head-Gordon, M.; Pople, J. A. A Direct MP2 Gradient-Method. *Chem. Phys. Lett.* **1990**, *166*, 275−280.
(64) Head-Gordon, M.; Rico, R. J.; Oumi, M.; Lee, T. J. A Doubles Correction to Electronic Excited-States from Configuration-Interaction in the Space of Single Substitutions. *Chem. Phys. Lett.* **1994**, *219*, 21−29.
(65) Krishnan, R.; Binkley, J. S.; Seeger, R.; Pople, J. A. Self-Consistent Molecular Orbital Methods. XX. A Basis Set for Correlated Wave Functions. *J. Chem. Phys.* **1980**, *72*, 650−654.
(66) Frisch, M. J.; Pople, J. A.; Binkley, J. S. Self-Consistent Molecular Orbital Methods 25. Supplementary Functions for Gaussian Basis Sets. *J. Chem. Phys.* **1984**, *80*, 3265−3269.
(67) Clark, T.; Chandrasekhar, J.; Spitznagel, G. W.; Schleyer, P. V. R. Efficient Diffuse Function-Augmented Basis Sets for Anion Calculations. III. The 3-21+G Basis Set for First-Row Elements, Li−F. *J. Comput. Chem.* **1983**, *4*, 294−301.
(68) Jeziorski, B.; Moszynski, R.; Szalewicz, K. Perturbation Theory Approach to Intermolecular Potential Energy Surfaces of Van Der Waals Complexes. *Chem. Rev. (Washington, DC, U. S.)* **1994**, *94*, 1887−1930.
(69) Jurecka, P.; Sponer, J.; Cerny, J.; Hobza, P. Benchmark Database of Accurate (MP2 and CCSD(T) Complete Basis Set Limit) Interaction Energies of Small Model Complexes, DNA Base Pairs, and Amino Acid Pairs. *Phys. Chem. Chem. Phys.* **2006**, *8*, 1985−1993.
(70) Flick, J. C.; Kosenkov, D.; Hohenstein, E. G.; Sherrill, C. D.; Slipchenko, L. V. Accurate Prediction of Noncovalent Interaction Energies with the Effective Fragment Potential Method: Comparison of Energy Components to Symmetry-Adapted Perturbation Theory for the S22 Test Set. *J. Chem. Theory Comput.* **2012**, *8*, 2835−2843.
(71) Slipchenko, L. V.; Gordon, M. S. Water−Benzene Interactions: An Effective Fragment Potential and Correlated Quantum Chemistry Study. *J. Phys. Chem. A* **2009**, *113*, 2092−2102.
(72) Parrish, R. M.; Burns, L. A.; Smith, D. G. A.; Simmonett, A. C.; DePrince, A. E.; Hohenstein, E. G.; Bozkaya, U.; Sokolov, A. Y.; Di Remigio, R.; Richard, R. M.; et al. Psi4 1.1: An Open-Source Electronic

DOI: 10.1021/acs.jpca.7b05875
J. Phys. Chem. A 2017, 121, 9495−9507

Structure Program Emphasizing Automation, Advanced Libraries, and Interoperability. *J. Chem. Theory Comput.* **2017**, *13*, 3185−3197.
(73) Hohenstein, E. G.; Sherrill, C. D. Wavefunction Methods for Noncovalent Interactions. *WIREs Comput. Mol. Sci.* **2012**, *2*, 304−326.
(74) Woon, D. E.; Dunning, T. H. Gaussian Basis Sets for Use in Correlated Molecular Calculations. IV. Calculation of Static Electrical Response Properties. *J. Chem. Phys.* **1994**, *100*, 2975−2988.
(75) Řezáč, J.; Hobza, P. Extrapolation and Scaling of the DFT-SAPT Interaction Energies toward the Basis Set Limit. *J. Chem. Theory Comput.* **2011**, *7*, 685−689.

DOI: 10.1021/acs.jpca.7b05875
J. Phys. Chem. A 2017, 121, 9495−9507